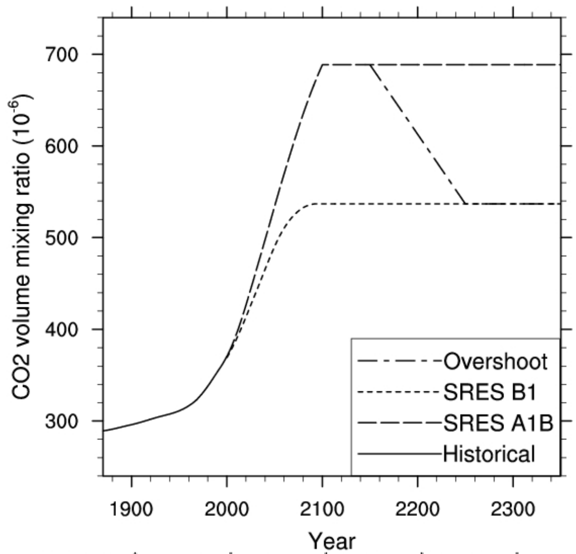


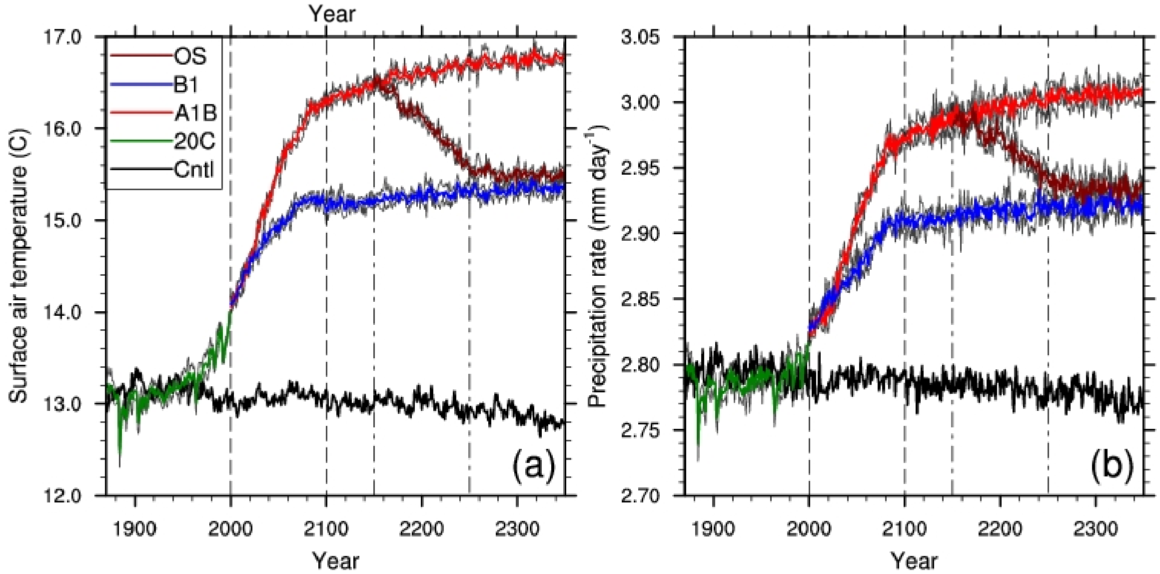


**Figure 10.5.11.** a) $CO_2$ concentrations for the overshoot experiment. b) globally averaged surface air temperatures for the overshoot scenario and the A1B and B1 experiments; c) globally averaged precipitation rate for the experiments in (a).

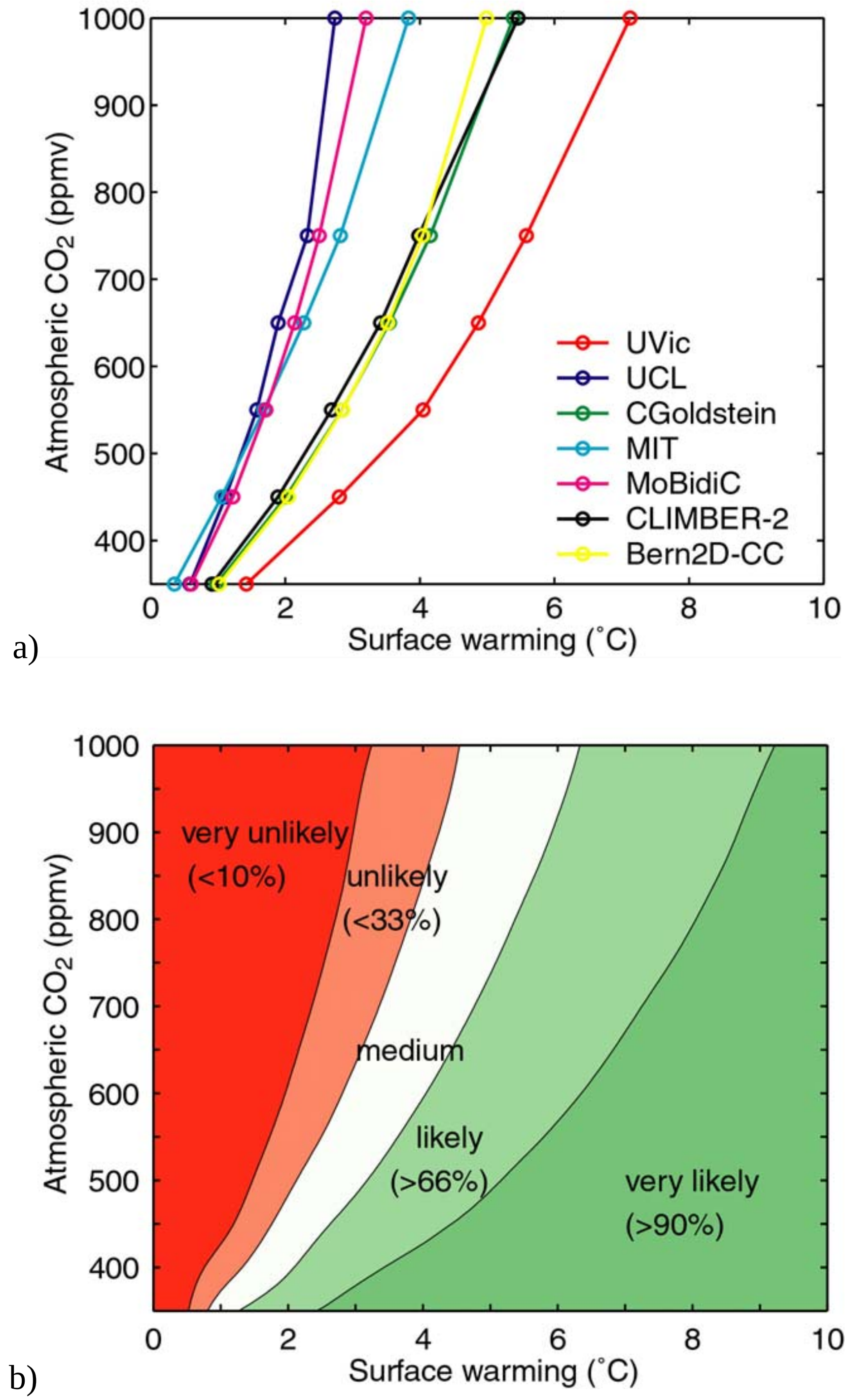


**Figure 10.5.12.** a) Equilibrium surface warming for seven different EMICs and different stabilization levels of atmospheric $CO_2$ or the equivalent radiative forcing, b) a probabilistic picture based on the same scenarios, showing probability of remaining below a certain warming threshold for a given $CO_2$ equivalent stabilization concentration, derived from one EMIC with variable ocean heat uptake and climate sensitivity.

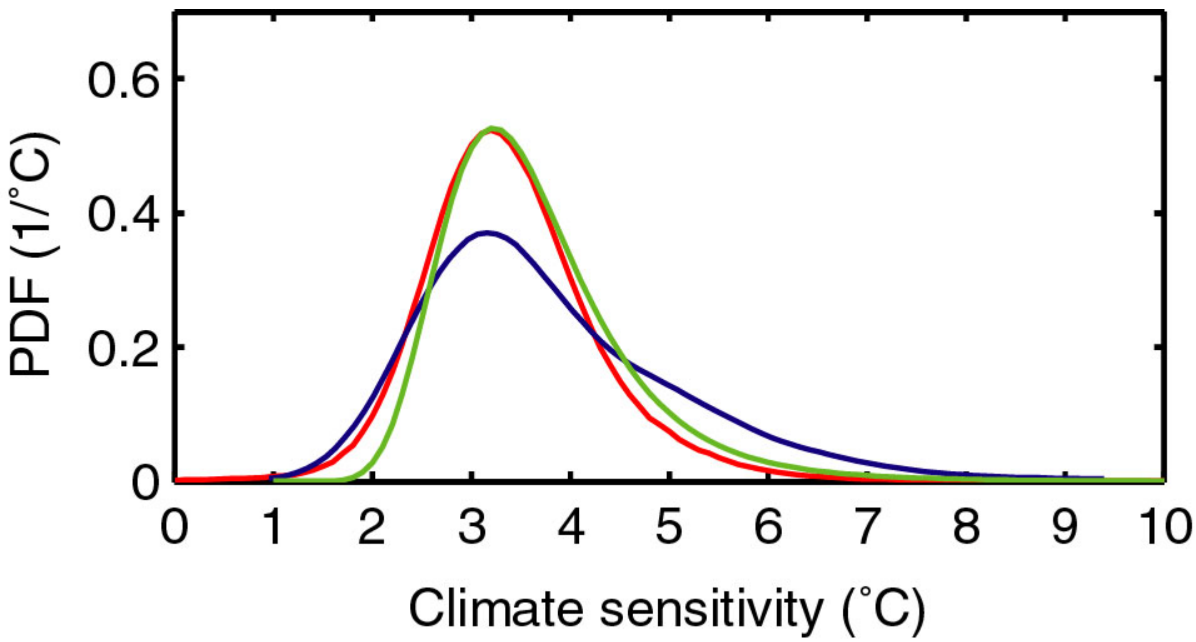


**Figure 10.5.13.** PDFs of climate sensitivity from Murphy et al. (2004)(green), Piani et al. (2005) (blue) and Knutti and Meehl (2005) (red). PDFs are truncated at 10°C.

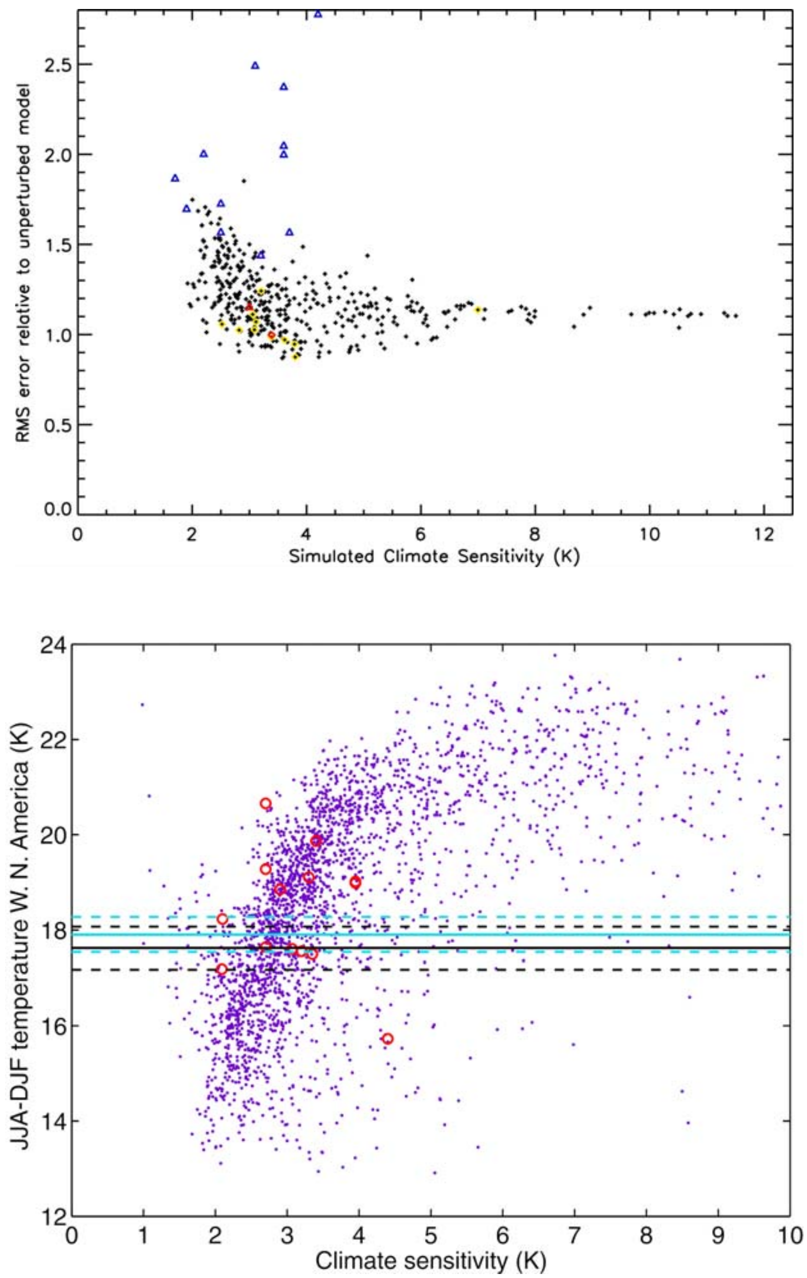


**Figure 10.5.14.** a) Values of climate sensitivity and relative model error from the perturbed physics ensemble of Stainforth et al. (2005). The red diamond shows the unperturbed model version, the yellow diamond shows model versions with only a single parameter perturbed and the black crosses show versions with multiple parameter perturbations. The triangles show results from members of the CMIP2 multi-model ensemble, with the value for HadCM3 (using the same atmosphere model as the unperturbed member of the perturbed physics ensemble, but with a dynamic rather than passive ocean), shown in red). Relative model error is calculated from the r.m.s. difference between simulated and observed climatological annual fields normalised by the value for the unperturbed model version, and averaged over the following variables: surface temperature, sea level pressure, precipitation, and surface sensible and latent heat flux. b) summer minus winter temperature over Western North America (dots) as a function of climate sensitivity, from the same Stainforth et al. (2005) dataset but using more simulations. The observed seasonal cycle and its uncertainty (solid and dashed lines, for both ERA40 and NCEP reanalysis) suggests that variables other than annual mean climate do constrain climate sensitivity. From Knutti and Meehl (2005).

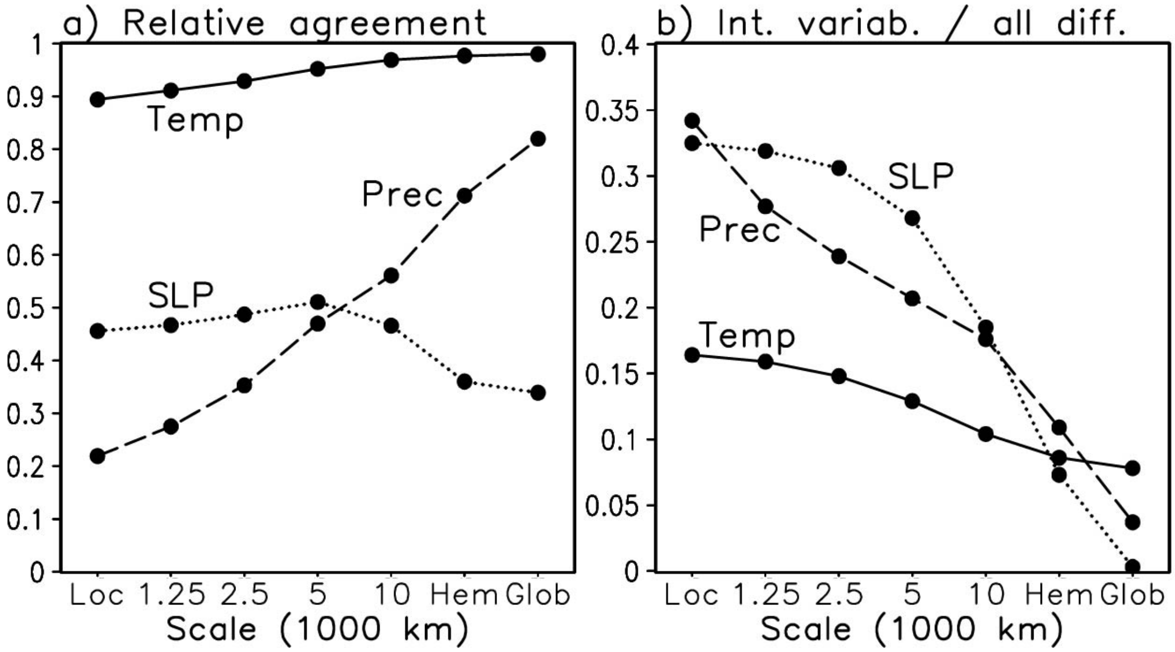


**Figure 10.5.15.** Statistics of annual mean responses from years 61–80 (time of $CO_2$ doubling) of a 15 member multimodel ensemble of transient climate change experiments (Räisänen, 2001), expressed as a function of horizontal scale ("Loc" = gridbox scale; "Hem" = hemispheric scale; "Glob" = global mean). The first panel shows the relative agreement between ensemble members, defined as the square of the ensemble-mean response (corrected to avoid sampling bias) divided by the mean squared response of individual ensemble members, and the second shows the contribution of internal variability to the ensemble variance of responses. Values are shown for surface air temperature, precipitation and sea level pressure.

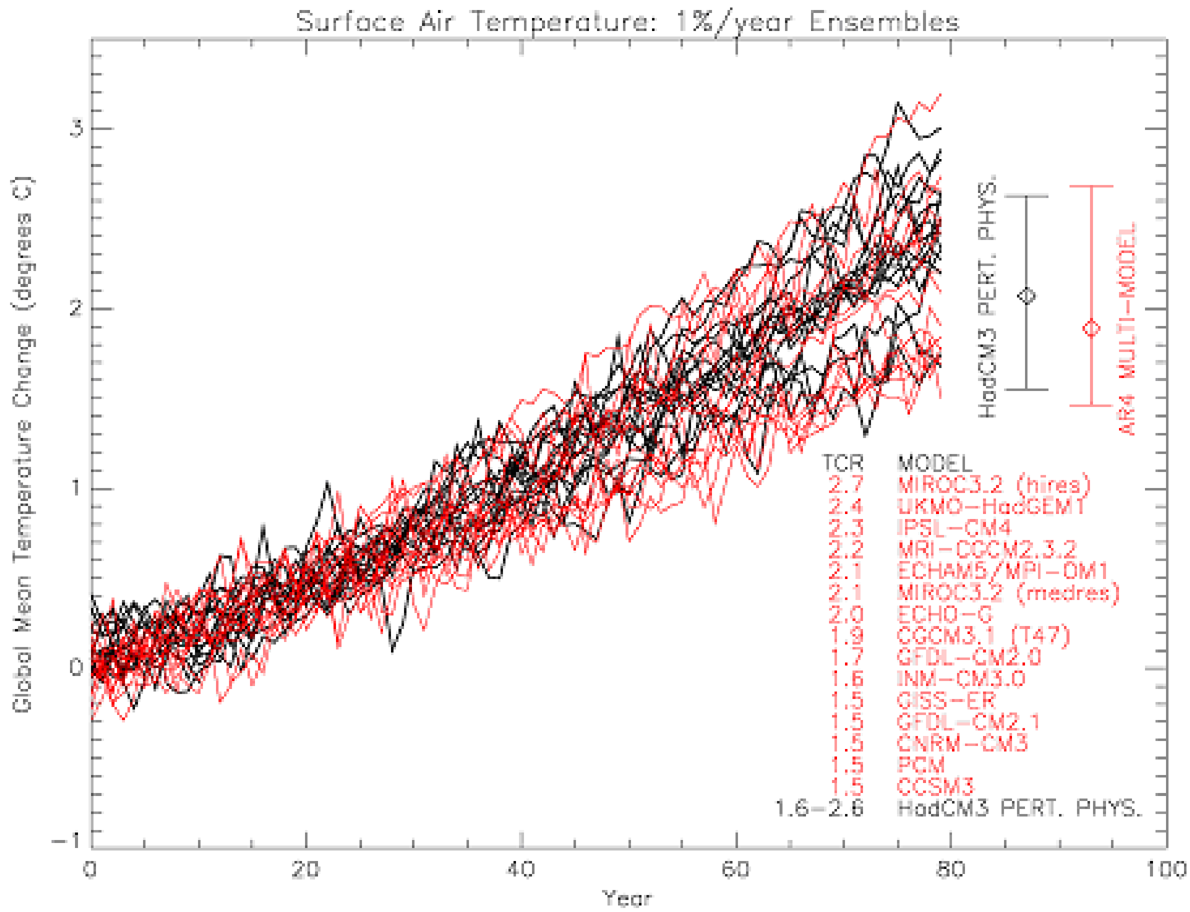


**Figure 10.5.16.** Response of global mean surface air temperature to a 1% per year increase in $CO_2$ from 17 member ensembles constructed from versions of the HadCM3 coupled ocean-atmosphere model with multiple perturbations to uncertain surface and atmospheric parameters (black lines) and coupled models comprising the AR4 multi-model ensemble (red lines). The mean and range of Transient Climate Response (TCR) for the two ensembles is indicated by the vertical bars and the table shows TCR values for multi-model ensemble members compared with the range from the HadCM3 perturbed physics ensemble. For the UKMO-HadGEM1 and MIROC3.2 hires models, only the scenario in which $CO_2$ concentrations are held fixed after year 70 were available, resulting in a likely but small underestimation of the model TCR.

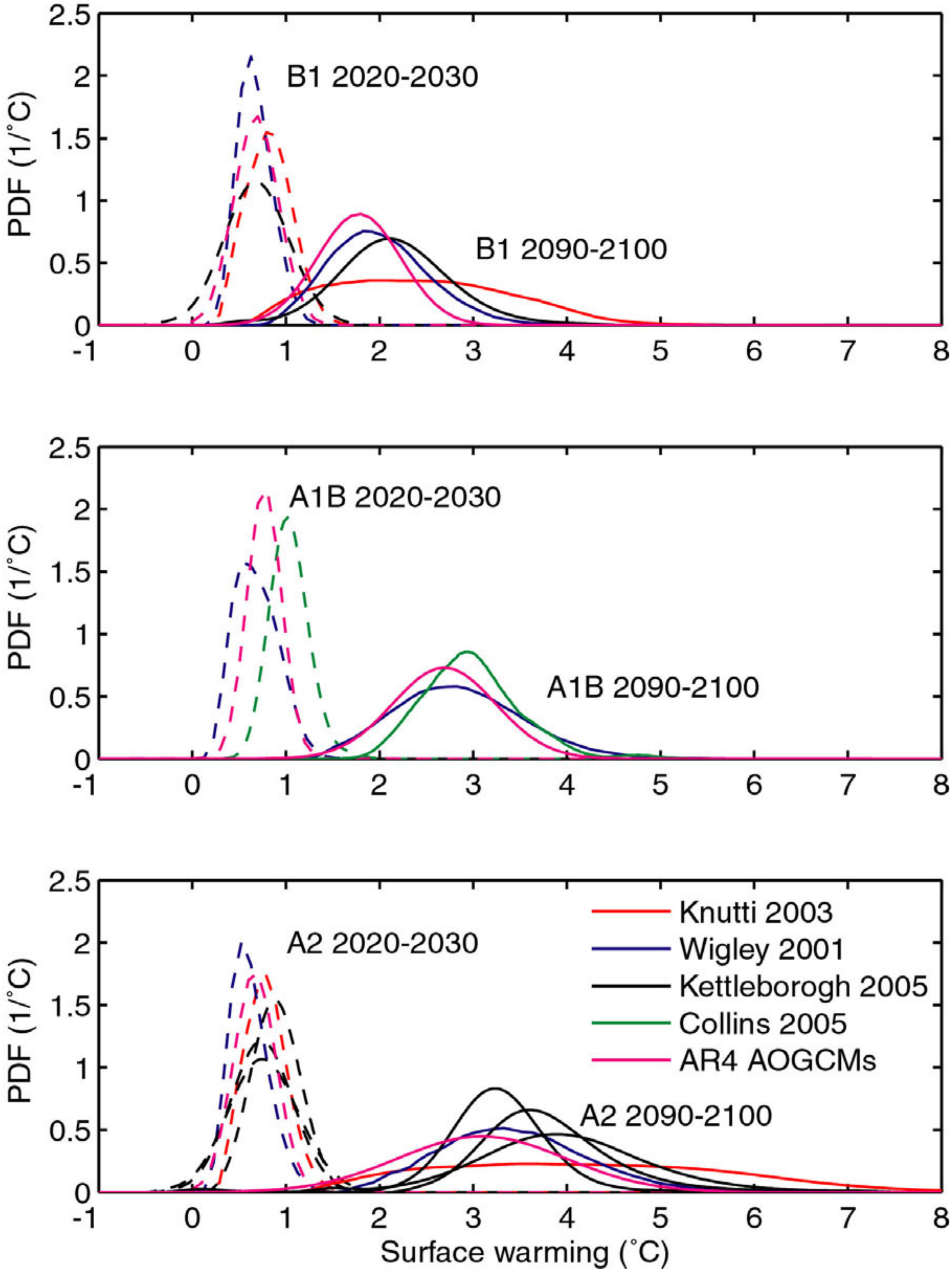


**Figure 10.5.17.** Probability density functions from different studies for global mean temperature change for the SRES scenarios B1, A1B and A2 and for the decades 2020–2030 and 2090–2100 relative to the 1980–2000 average. A normal fit to the multi-model ensemble is given for comparison.
See text for details.

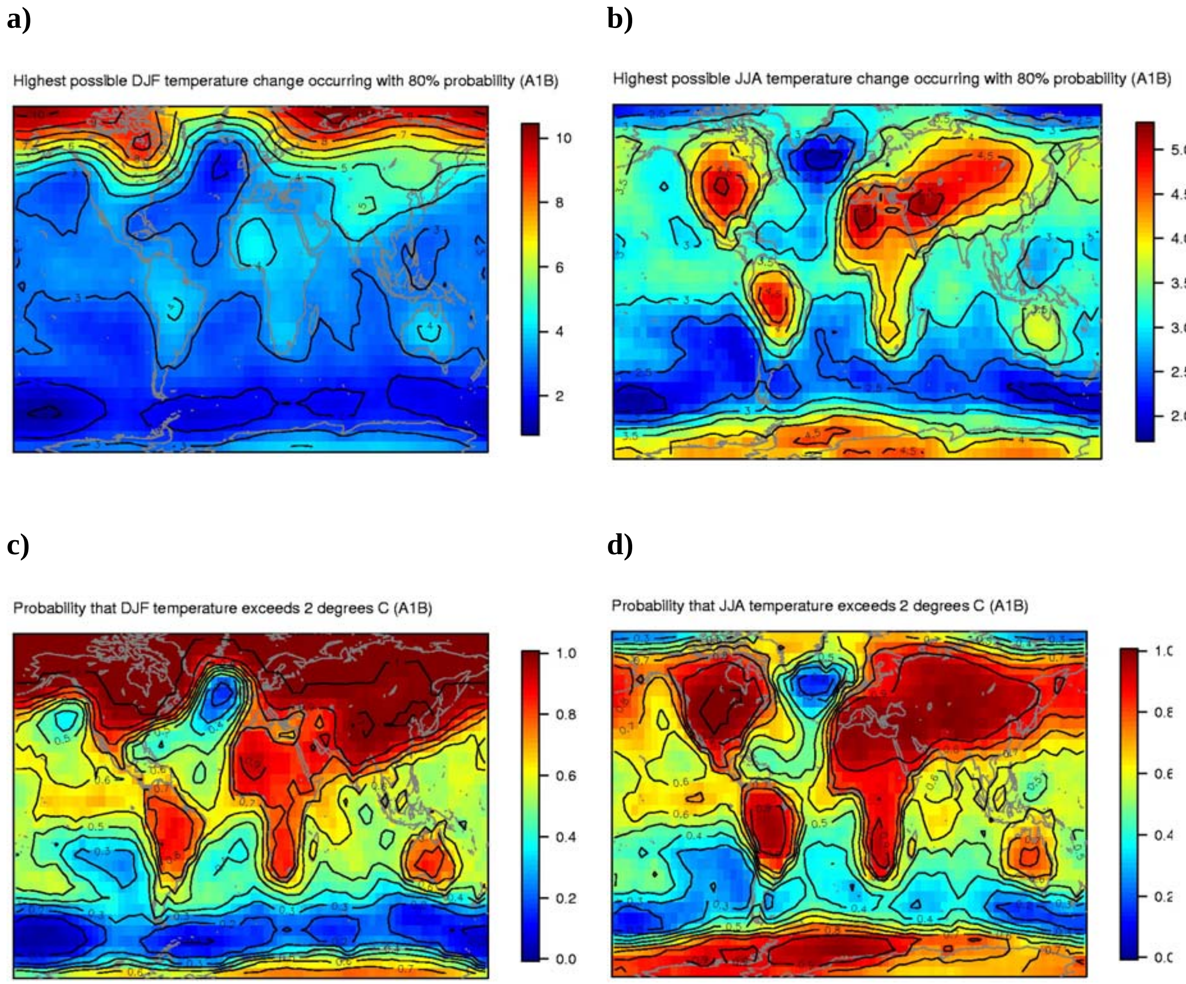


**Figure 10.5.18.** Using the Furrer et al. (2005) method, a) The highest temperature changes that have an 80% probability of occurrence by the end of the 21st century for the A1B scenario from an 21 member multi-model AOGCM ensemble for DJF (one ensemble member for each model); b) same as (a) except for JJA; c) probabilities of occurrence of at least a 2°C warming by the end of the 21st century for the A1B scenario for DJF for the same models as in (a); d) same as (c) except for JJA. To facilitate the calculations, the model data has first been interpolated to a 500 km grid.

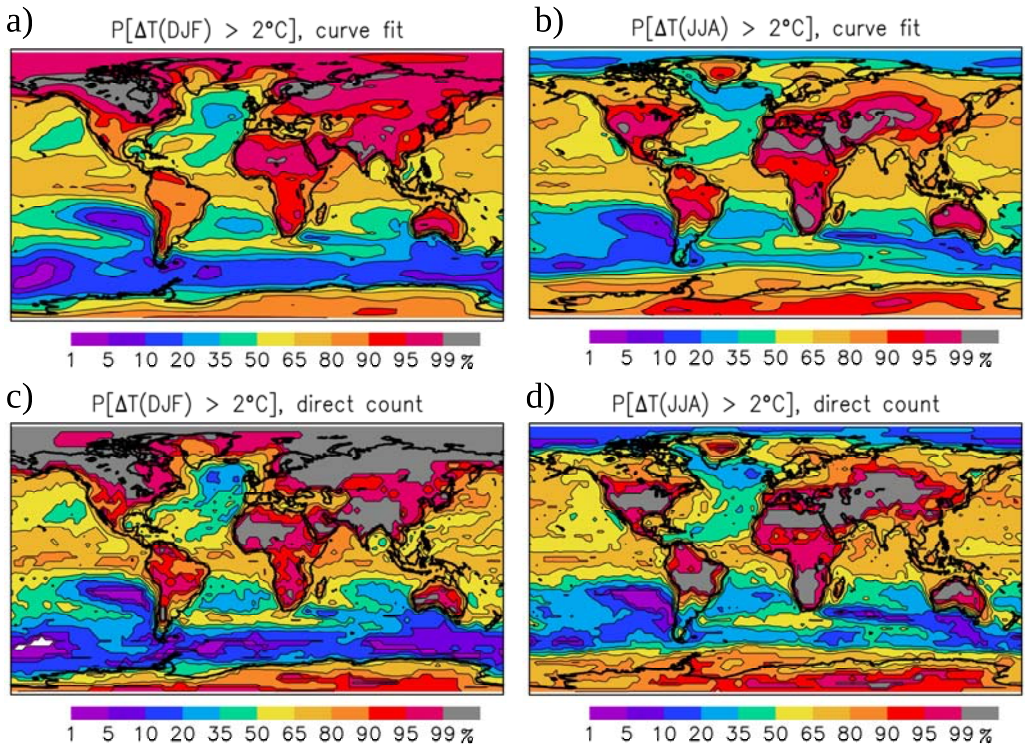


**Figure 10.5.19.** a) Using the Räisänen (2005b) method with a 21 member multi-model AOGCM ensemble (one ensemble member for each model), probabilities of occurrence of at least a 2°C warming by the end of the 21st century for the A1B scenario for DJF; b) same as (a) except for JJA; c) using the same 21 models as in (a), the percent of models at each grid point that produce at least 2°C warming for DJF; d) same as (c) except for JJA. Resolution for these calculations is about 250 km.

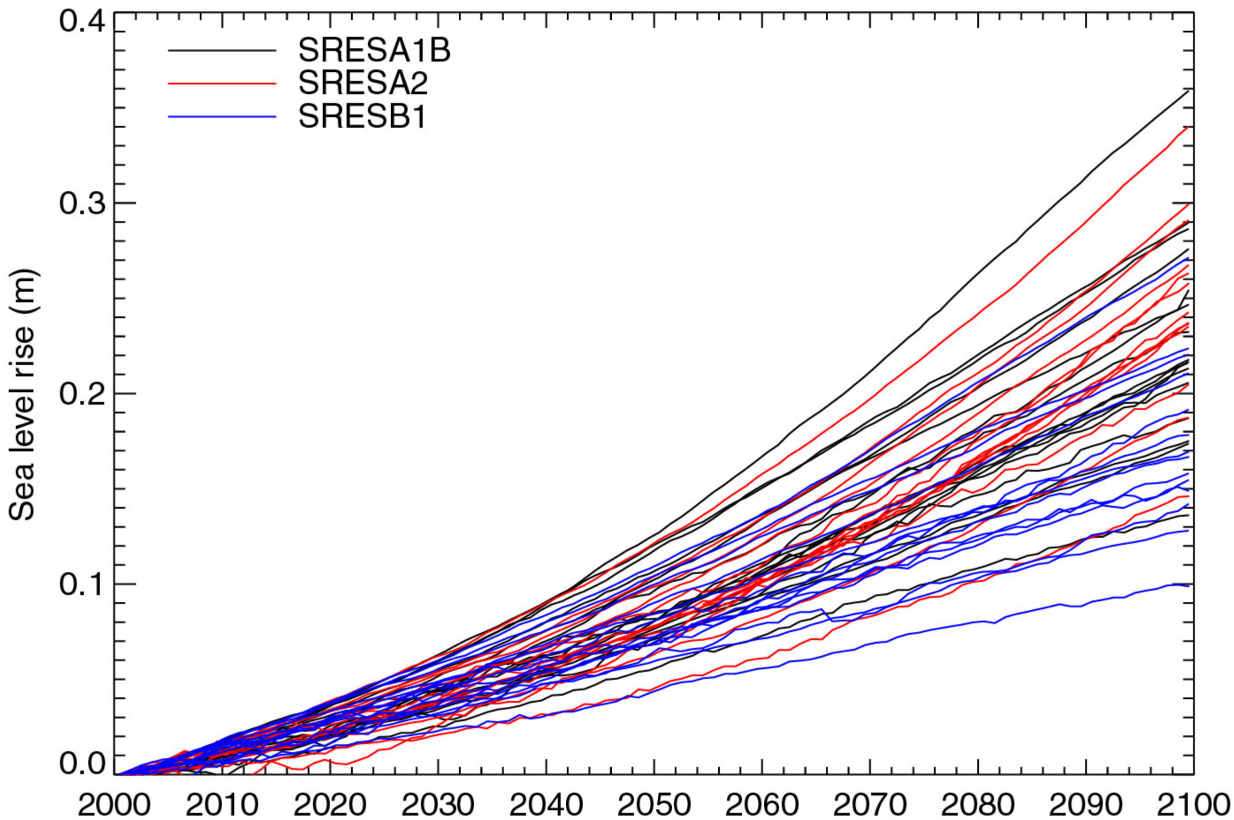


**Figure 10.6.1.** Global average sea level rise (m) due to thermal expansion during the 21st century relative to 2000 under SRES scenarios calculated from 16 AOGCMs (CCSM3, CGCM3.1 T47, CNRM-CM3, CSIRO-Mk3.0, ECHAM5/MPI-OM, GFDL-CM2.0, GFDL-CM2.1, GISS-AOM, GISS-EH, GISS-ER, INM-CM3.0, MIROC3.2 hires, MIROC3.2 medres, MRI-2.3.2a, PCM1, UKMO-HadCM3)

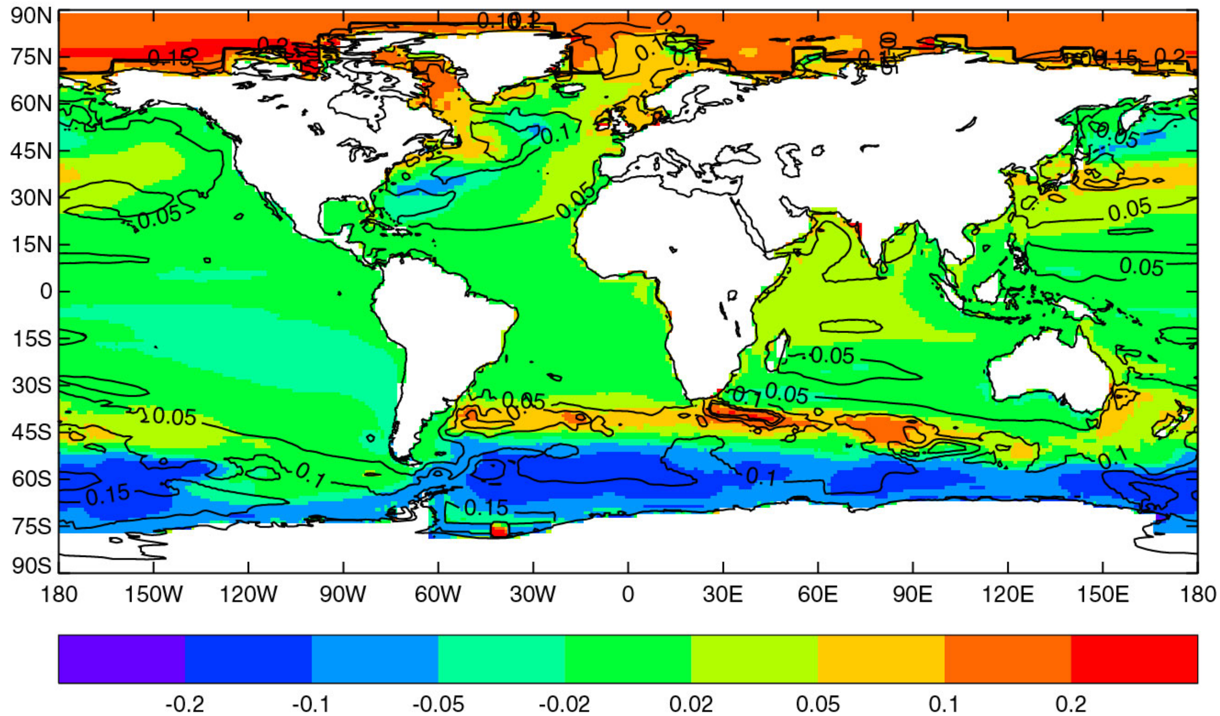


**Figure 10.6.2.** Local sea level change (m) due to ocean density and circulation change relative to the global average (i.e. positive values indicate greater local sea level change than global) during the 21st century, calculated as the difference between averages for 2080–2100 and 1980–2000 under SRES scenario A1B, as an ensemble mean over 14 AOGCMs (BCCR-BCM2.0, CGCM3.1 T47, CSIRO-Mk3.0, ECHAM5/MPI-OM, FGOALS-g1.0, GISS-AOM, GISS-EH, GISS-ER, IPSL-CM4, MIROC3.2 hires, MIROC3.2 medres, MRI-2.3.2a, UKMO-HadCM3, UKMO-HadGEM1). Contour lines show the intraensemble standard deviation.

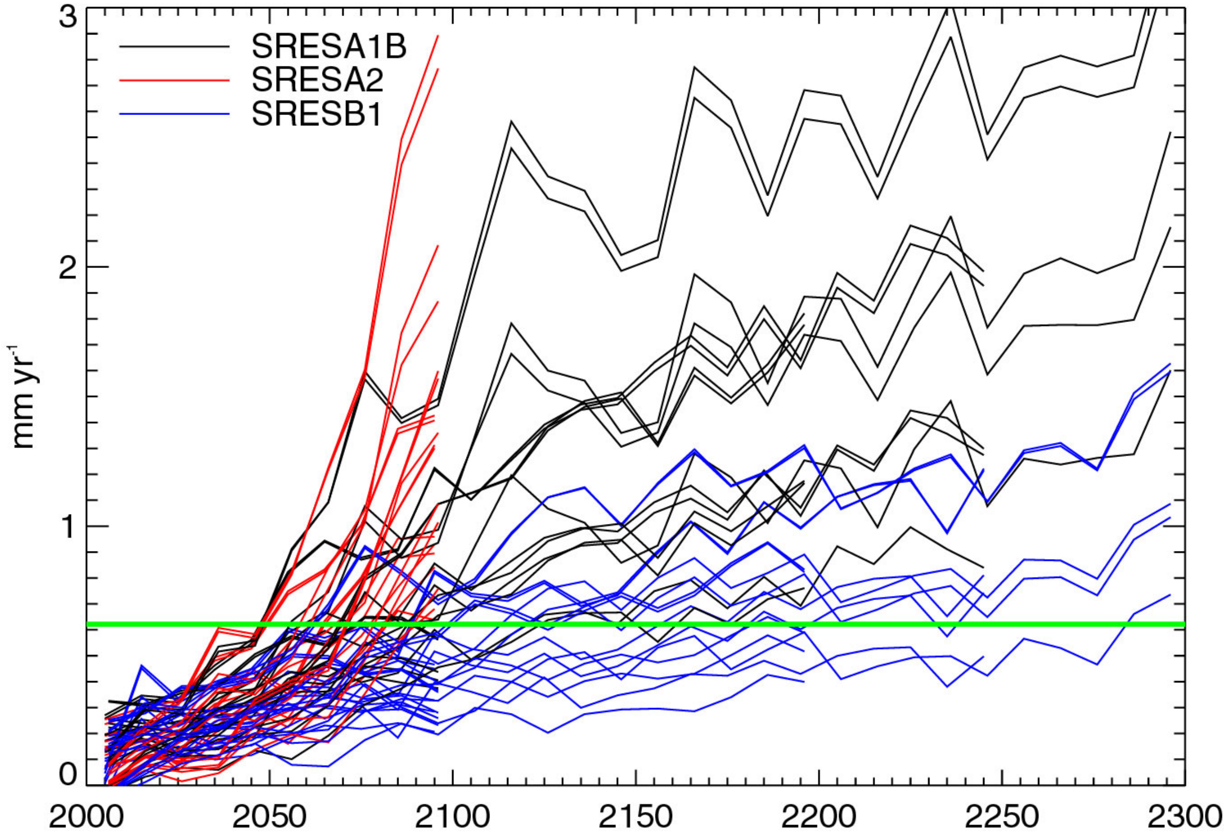


**Figure 10.6.3.** Increase in rate of net surface ablation, expressed as sea level rise equivalent, from the Greenland ice sheet under SRES scenarios with stabilisation of atmospheric concentrations at 2100, using results from 18 AOGCMs, following Gregory et al. (2005). Dynamic response is excluded. The horizontal green line indicates the present-day net surface mass balance of the ice sheet (Church et al., 2001). When the increase in surface ablation rises above this line, the net mass balance of the ice sheet is negative even with calving reduced to zero.

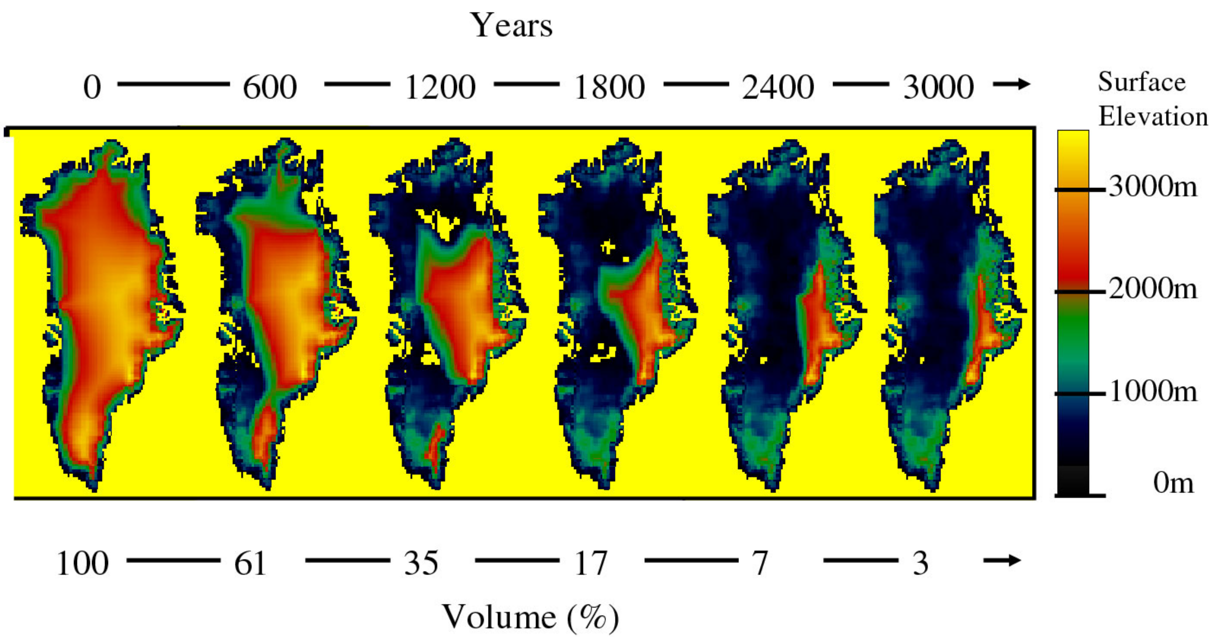


**Figure 10.6.4.** Evolution of Greenland surface elevation and ice sheet volume (lower scale) in the experiment of Ridley et al. (2005) with the HadCM3 AOGCM coupled to the Greenland ice sheet model of Huybrechts and De Wolde (1999) under a climate of constant 4 × preindustrial $CO_2$.

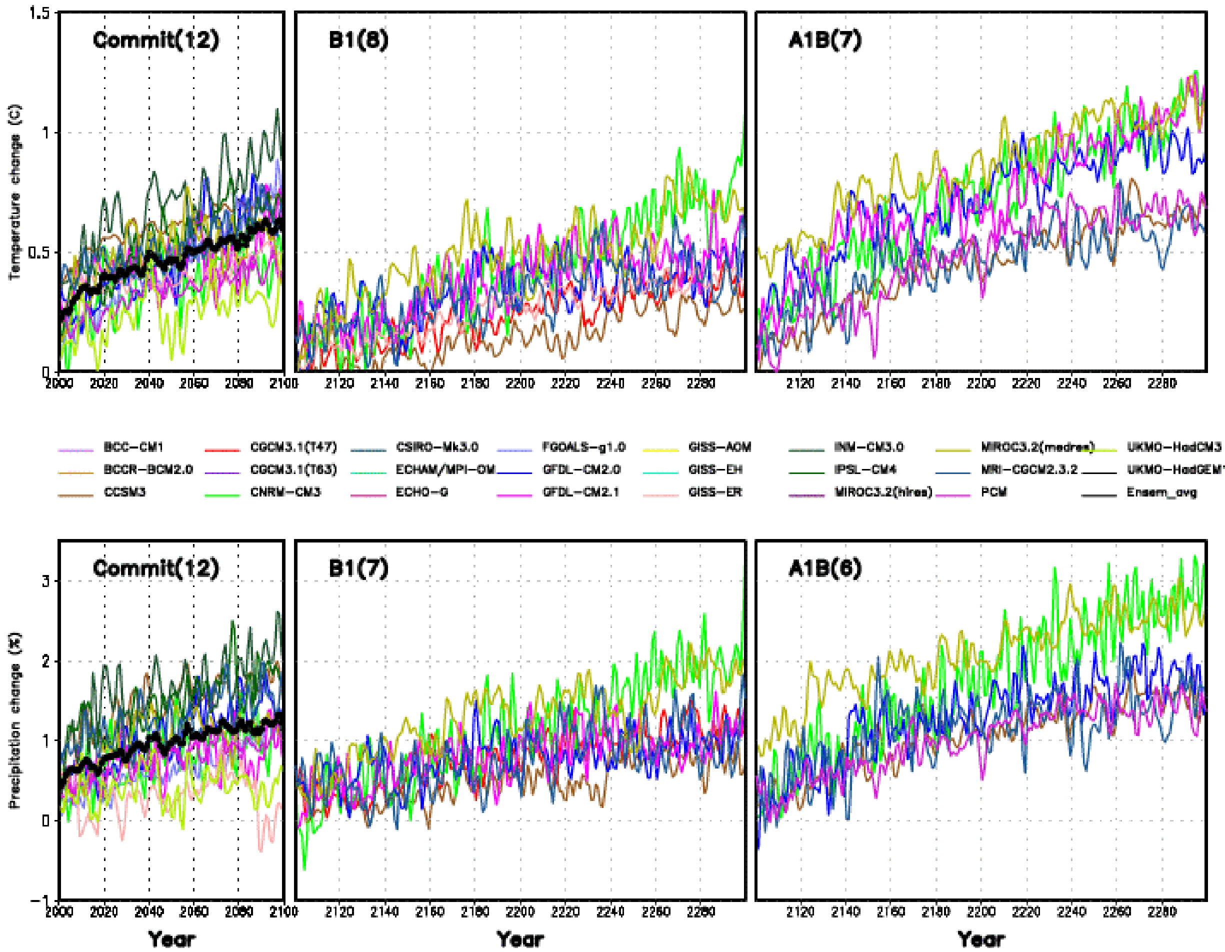


**Figure 10.7.1.** Top left: Globally averaged surface air temperature change computed with respect to 1980–1999 for the 20th century commitment experiment; Top center: Same as left except for the B1 commitment experiment computed with respect to the 2080–2099 average; Top right: Same as center except for the A1B commitment experiment; Bottom left: Same as top left except for percent change in globally averaged precipitation; Bottom center: Same as top center except for percent change in globally averaged precipitation; Bottom right: Same as top right except for percent change in globally averaged precipitation.

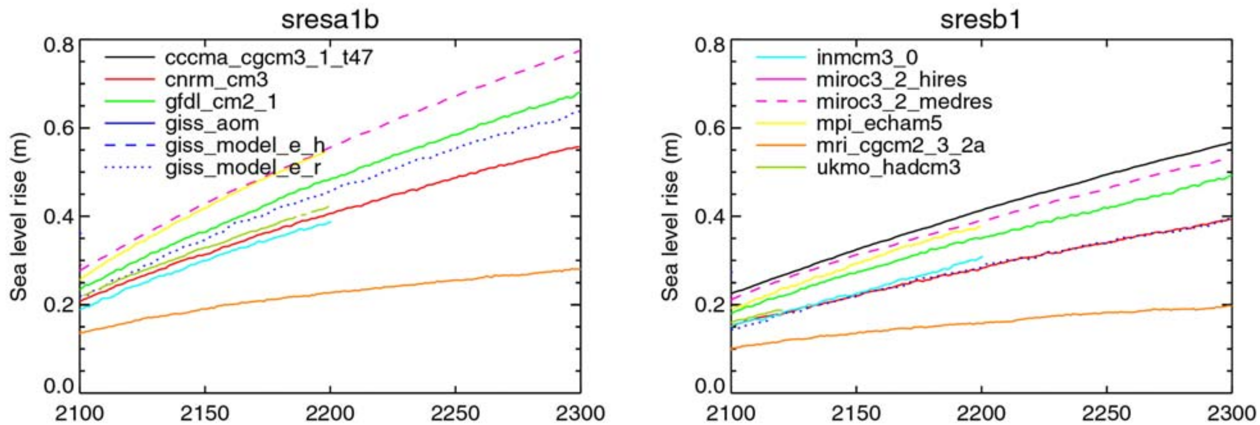


**Figure 10.7.2.** Globally averaged sea level change from thermal expansion for the A1B (left) and B1 (right) commitment experiment calculated from AOGCMs.

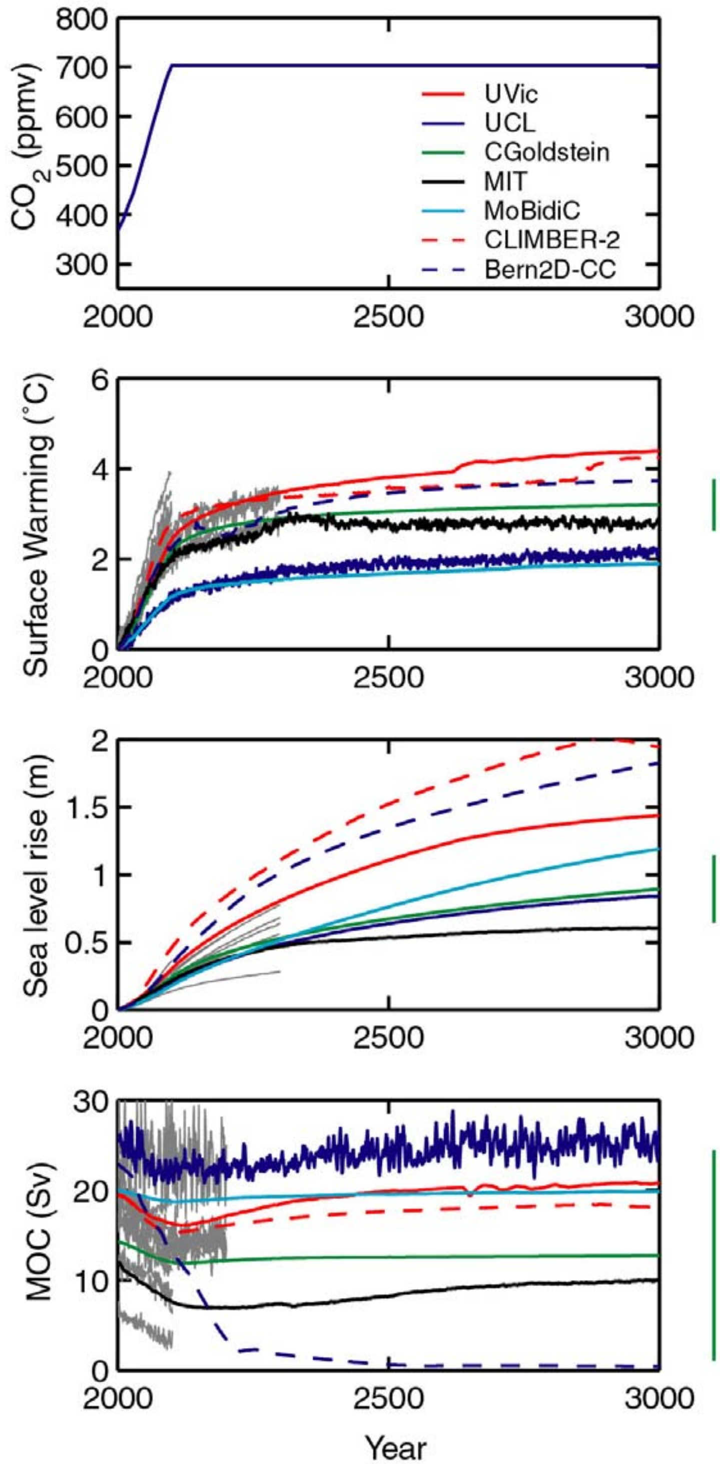


**Figure 10.7.3** a) atmospheric $CO_2$, b) global mean surface warming, c) sea level rise from thermal expansion and d) Atlantic meridional overturning circulation for the SRES A1B scenario and stable radiative forcing after 2100, showing long-term commitment after stabilization. Coloured lines are results from intermediate complexity models, grey lines indicate AOGCM results where available for comparison. Vertical bars indicate plus/minus two standard deviation uncertainties due to ocean parameter perturbations in the Goldstein model. The MOC shuts down in the Bern model, leading to an additional contribution to sea level rise.

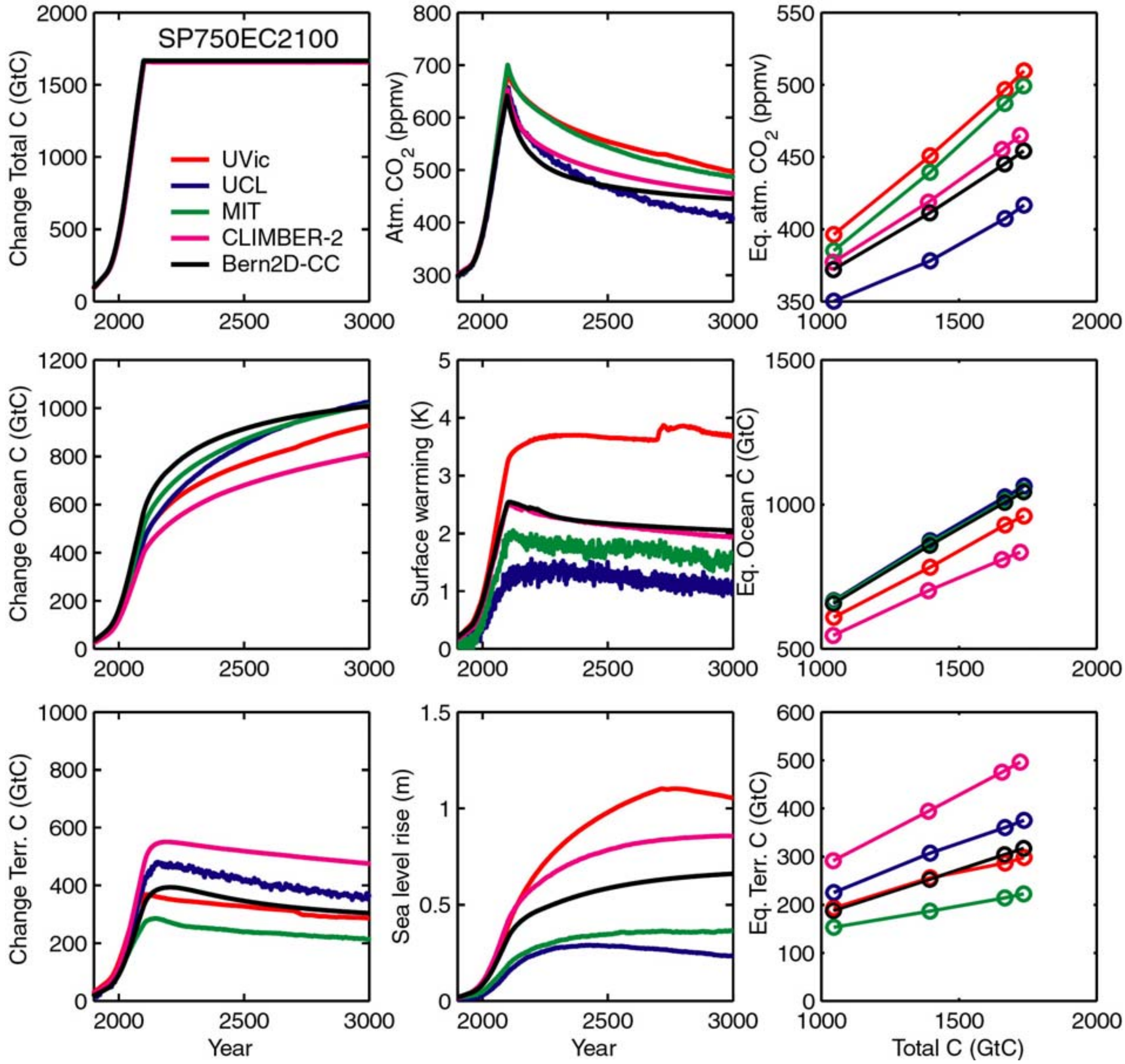


**Figure 10.7.4.** Left column: change in total, ocean and terrestrial carbon inventory from preindustrial for five different intermediate complexity models and a scenario where emissions follow a pathway leading to stabilization of atmospheric $CO_2$ at 750 ppmv, but before reaching this target, emissions are reduced to zero instantly at year 2100. Middle column: atmospheric $CO_2$ and climatic response of surface warming and sea level rise due to thermal expansion for the same scenario. Right column: Atmospheric $CO_2$, oceanic and terrestrial carbon uptake from preindustrial at year 3000 for several emission scenario of this type but with different total carbon emissions.

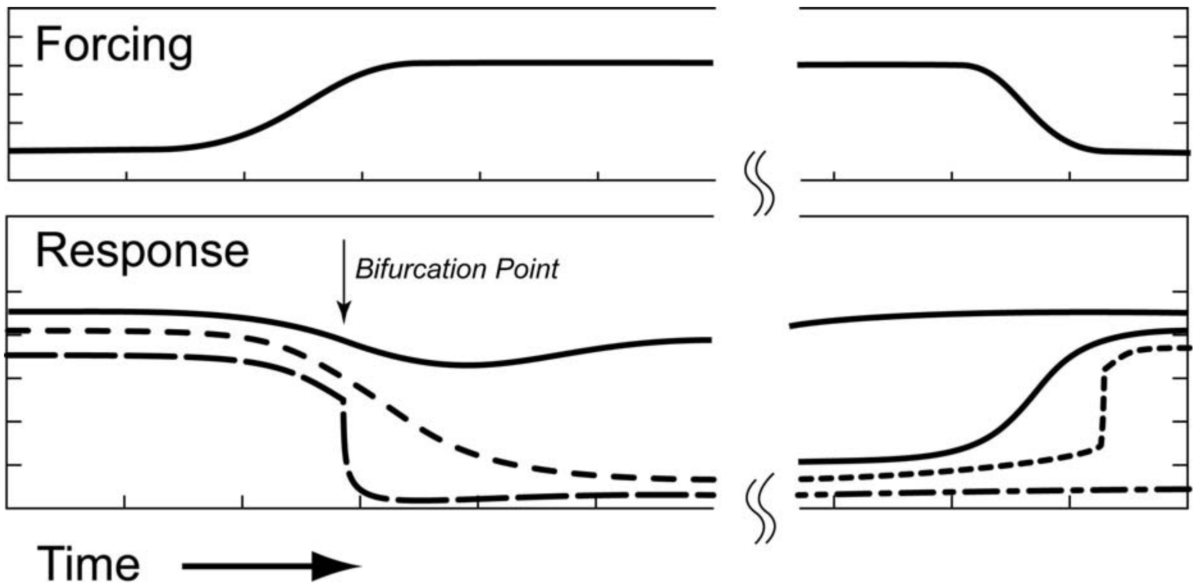


**Box 10.1, Figure 1.** Schematic illustration of various responses of a climate variable to forcing. The forcing (top panels) reaches a new stable level (left part of figure), and later approaches the original level on very long time scales (right part of the figure). The response of the climate variable (bottom panels) can be smooth (solid line) or cross a bifurcation point inducing a transition to a structurally different state (dashed lines). That transition can be rapid (abrupt change, long-dashed), or gradual (short-dashed), but is usually dictated by the internal dynamics of the climate system rather than the forcing. The long-term behaviour (right panel) also exhibits different possibilities. Changes can be irreversible (dash-dotted) with the system settling at a different, stable state, or reversible (solid, dotted) when the forcing is set back to its original value. In the latter case, the transition can, again, be gradual or abrupt. One example for the illustration, but not limited to, is the response of the Atlantic meridional overturning circulation to a gradual change in radiative forcing.

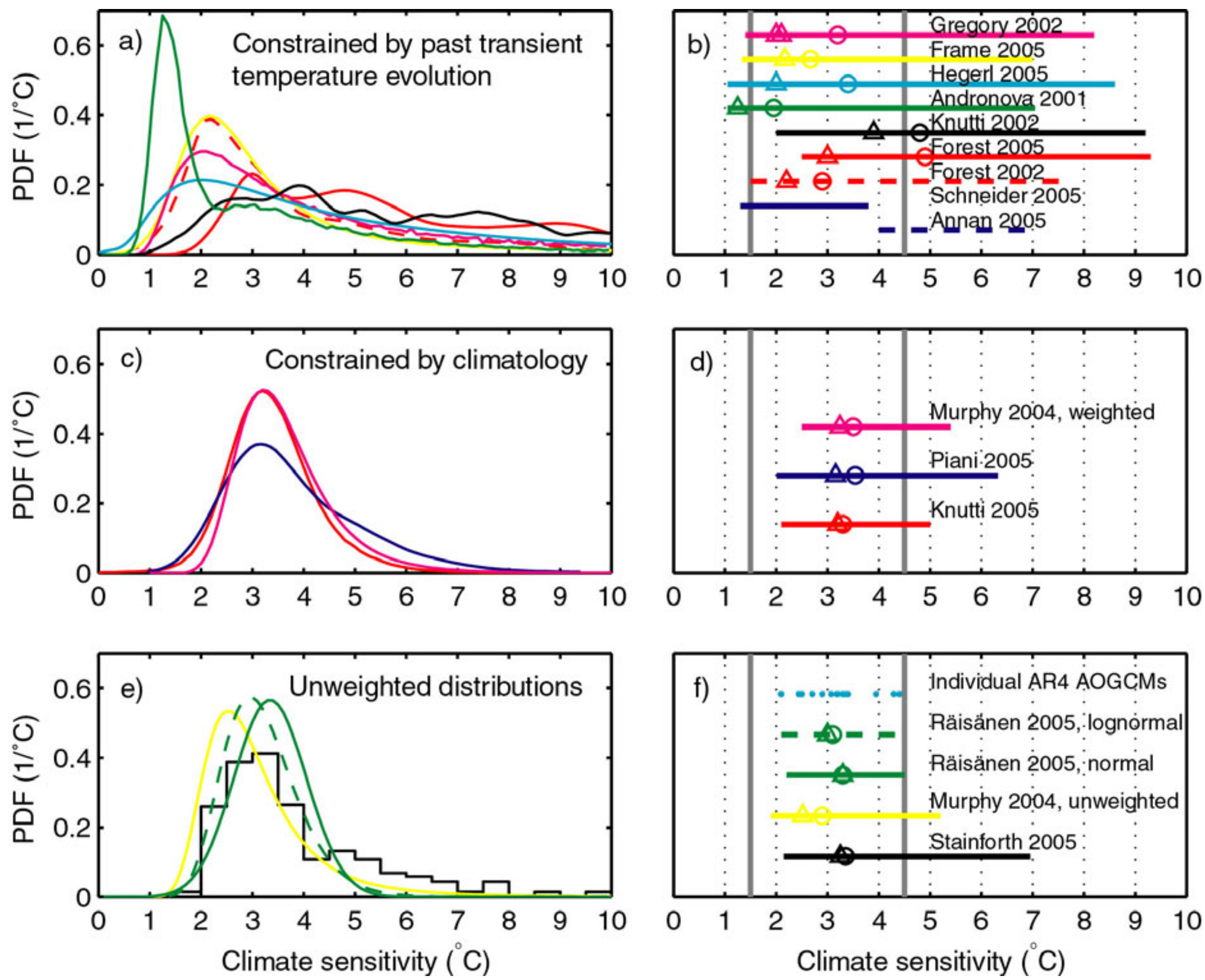


**Box 10.2, Figure 1.** a) PDFs constrained by the transient evolution of the atmospheric temperature, radiative forcing and ocean heat uptake, b) as in panel a) but 5–95% ranges, medians (circles) and maximum probabilities (triangles), c/d) same but using constraints from present-day climatology, e/f) unweighted or fitted distributions from different models or from perturbing parameters in a single model. See text for details. Vertical grey lines mark the range of 1.5–4.5°C given in the TAR (2001). All PDFs are truncated at 10°C for consistency, ranges may differ from numbers reported in individual studies.

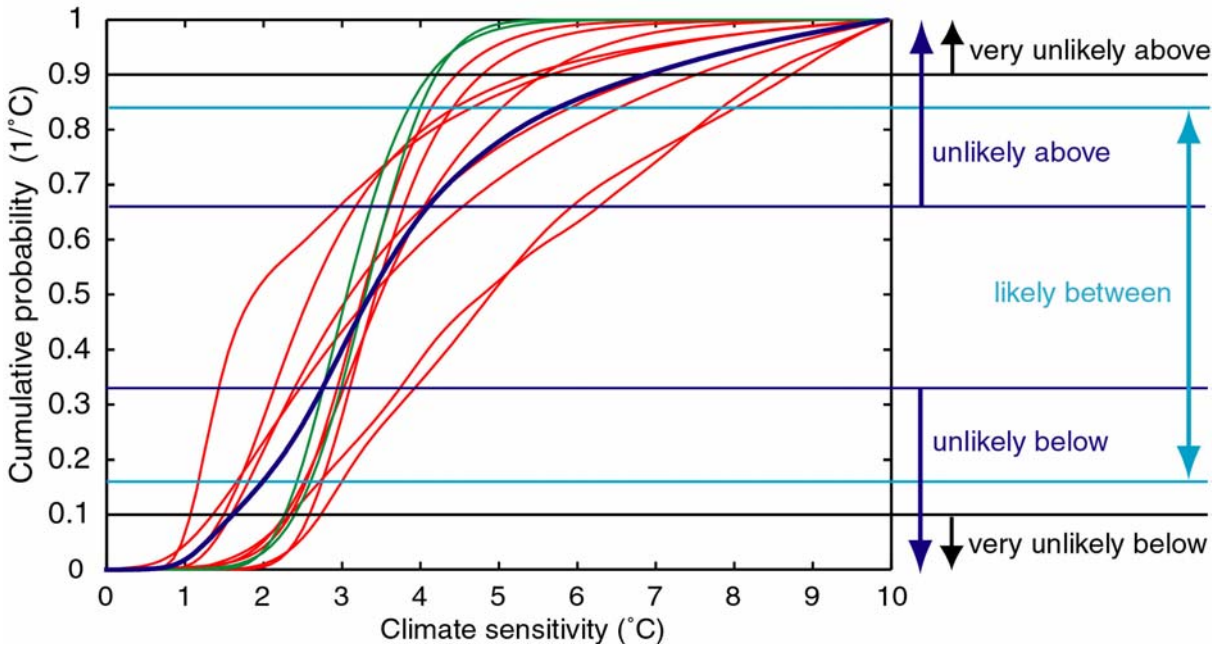


**Box 10.2, Figure 2.** Individual cumulative distributions of climate sensitivity (red) and their average (blue) from Box 10.2, Figure 1a/c (except LGM studies and Forest et al. (2002) which is superseded by Forest et al. (2005)) and cumulative distributions fitted to the AOGCMs climate sensitivities (green) from Figure 10.2.1e. Horizontal lines and arrows mark the edges of the likelihood estimates according to AR4 guidelines.